Correlation between composition and structure in boracites

2007 J. Phys.: Condens. Matter 19 275207

(http://iopscience.iop.org/0953-8984/19/27/275207)

IOP PUBLISHING JOURNAL OF PHYSICS: CONDENSED MATTER

J. Phys.: Condens. Matter **19** (2007) 275207 (16pp) doi:10.1088/0953-8984/19/27/275207

Correlation between composition and structure in boracites

K Knorr[1], L Peters[1,5], B Winkler[2], V Milman[3] and A G Castellanos-Guzman[4]

[1] Christian-Albrechts Universität zu Kiel, Institut für Geowissenschaften, Mineralogie, Olshausenstraße 40, D 24098 Kiel, Germany
[2] Johann Wolfgang Goethe Universität, Mineralogie Kristallographie, Senckenberganlage 30, D 60054 Frankfurt am Main, Germany
[3] Accelrys Incorporated, 334 Science Park, Cambridge CB4 0WN, UK
[4] LIM.DIP Cucei Universidad de Guadalajara, Apartado Postal 2-638, 44281 Guadalajara Jal., Mexico

E-mail: knorr@min.uni-kiel.de

Received 22 December 2006
Published 1 June 2007
Online at stacks.iop.org/JPhysCM/19/275207

Abstract

In a combined x-ray diffraction and density functional theory based study the bonding properties of several halogenide boracites have been investigated. We show that DFT calculations reliably reproduce the small spontaneous deformations of non-cubic boracites and that they therefore can be used to predict pressure-induced structural changes. Specifically, we predict the compressibility and the pressure-induced deformation of Mg–Cl boracite. Earlier findings concerning an unusual bond length in Co–Cl boracite are challenged. The arrangement of the halogenide ions and metal cations along chains running through the structure is rationalized in terms of electronegativity differences. We also show that the substitution of the halogenide or metal ions has no significant effect on the B–O bonds.

1. Introduction

Boracites are a very interesting class of compounds, as they display a variety of ferroic phase transitions and have interesting dielectric, magnetic and optical properties. Halogenide boracites have the general formula $M_3[B_7O_{13}]X$, where M represents a divalent metal and X is a halogen ion (F, Cl, Br or I). Throughout this paper, the composition of a boracite is denoted by the abbreviation M–X with M and X the chemical symbols of the respective metal and halogenide atoms. The ferroic phase transitions of boracites have been thoroughly discussed in the framework of Landau theory (e.g. Dvorak 1971, Dvorak and Petzelt 1971, Toledano *et al* 1985). During these phase transitions, the symmetry usually decreases with decreasing

[5] Present address: Chemistry Department, Science Laboratories, University of Durham, South Road, DH1 3LE, UK.

temperature from cubic (mostly $F\bar{4}3c$) to orthorhombic $Pca2_1$ or through a monoclinic intermediate step to rhombohedral $R3c$, but other space group symmetries have also been observed. Despite the numerous previous studies, some results reported in the literature raise questions with respect to structural details. Here, we address the structure and bonding in some halogenide boracites by an experimental study and quantum mechanical model calculations, which allow a deeper understanding of structure–property relations in this class of compounds.

Before discussing individual aspects of the structural behaviour of boracites, it is worthwhile to summarize some general structural features of the boracite structure in order to introduce the nomenclature. In cubic boracites (e.g. Sueno *et al* 1973) the M and X atoms form a three dimensional net of –X–M–X–M–X– chains with an M–X distance of about 3 Å along the $\bar{4}$-axis of space group $F\bar{4}3c$. The chains intersect at the X atom sites. B and O form a three-dimensional connected network of BO_4 and OBO_3 groups. The BO_4 group is a tetrahedron with B1 on a $\bar{4}$-axis, while the B2 atom in the OBO_3 group is displaced from the centre of the tetrahedron along the threefold axis towards three symmetrically equivalent oxygen atoms (O2). This results in different B2–O bond lengths: three distances to O2 of about 1.44 Å and a stretched bond to O1 of about 1.7 Å. The coordination around the M ion is pseudo-octahedral, with four oxygen atoms in the equatorial plane and two X atoms at the apices (figure 1(a)). The parameter ε [Å] $= x(\mathrm{O1}) \cdot a$ [Å] (Nelmes and Hay 1981) describes the displacement of the O1 atoms from a plane whose location is chosen such that the M ion is contained and the distances to the oxygen atoms are minimal. O1 is coordinated by boron B2 in the form of a regular tetrahedron (figure 1(b)). In trigonal boracite this tetrahedron is deformed into a trigonal pyramid plus one B atom at a longer distance. Furthermore, it is assumed that there is no B2–O1 bond, and hence the coordination of B2 is almost planar trigonal. At the cubic to trigonal or orthorhombic phase transition the geometry of the M–X chains changes dramatically (e.g. Dowty and Clark 1973). The M coordination is fivefold and represents a transition between square pyramidal and trigonal bipyramidal with the oxygen atoms constituting the base plane of the pyramid and X located at the apex. Note that the base plane is distorted. As a consequence, the equivalent distances in the M–X chains become inequivalent, and the chains are then formed by M–X pairs linked together through long X . . . M contacts. Typical M–X distances are about 2.5–2.6 Å for the short distance while the long X . . . M distances are longer than 3.0 Å. The X . . . M–X . . . M–X . . . chains are not longer straight but kinked (figure 1(c)). The structures of the rhombohedral $R3c$ and the orthorhombic $Pca2_1$ phases are very similar (Dowty and Clark 1973).

The symmetry of the *para*-phase of boracite is $F\bar{4}3m$, with conventional lattice vectors $\boldsymbol{a}_1^{\mathrm{c}}$, $\boldsymbol{a}_2^{\mathrm{c}}$, $\boldsymbol{a}_3^{\mathrm{c}}$, where the index c denotes the conventional cubic cell. The phase transitions lead to spontaneous deformations. Since the orientation of ferroelastic domains does not change the magnitude of the spontaneous strain, the lattice vectors of only one domain of the ferroelastic low symmetry phases are discussed. The lattice parameters of orthorhombic boracite (index o) with space group $Pca2_1$ are related to the cubic cell by

$$\boldsymbol{a}_1^{\mathrm{o}} = (\boldsymbol{a}_1^{\mathrm{c}} + \boldsymbol{a}_2^{\mathrm{c}})/2, \qquad \boldsymbol{a}_2^{\mathrm{o}} = (-\boldsymbol{a}_1^{\mathrm{c}} + \boldsymbol{a}_2^{\mathrm{c}})/2, \qquad \text{and} \qquad \boldsymbol{a}_3^{\mathrm{o}} = \boldsymbol{a}_3^{\mathrm{c}}. \tag{1}$$

We calculate a scalar orthorhombic spontaneous strain from the magnitudes of the orthorhombic lattice parameters by

$$e^{\mathrm{o}} = 4|a_1^{\mathrm{o}} - a_2^{\mathrm{o}}|/(a_1^{\mathrm{o}} + a_2^{\mathrm{o}}). \tag{2}$$

For the characterization of the spontaneous deformation of the rhombohedral phase of boracite we make use of the primitive lattice of the cubic cell, which is

$$\boldsymbol{a}_1^{\mathrm{cp}} = (\boldsymbol{a}_1 + \boldsymbol{a}_2)/2, \qquad \boldsymbol{a}_2^{\mathrm{cp}} = (\boldsymbol{a}_2 + \boldsymbol{a}_3)/2, \qquad \text{and} \qquad \boldsymbol{a}_3^{\mathrm{cp}} = (\boldsymbol{a}_1 + \boldsymbol{a}_3)/2 \tag{3}$$

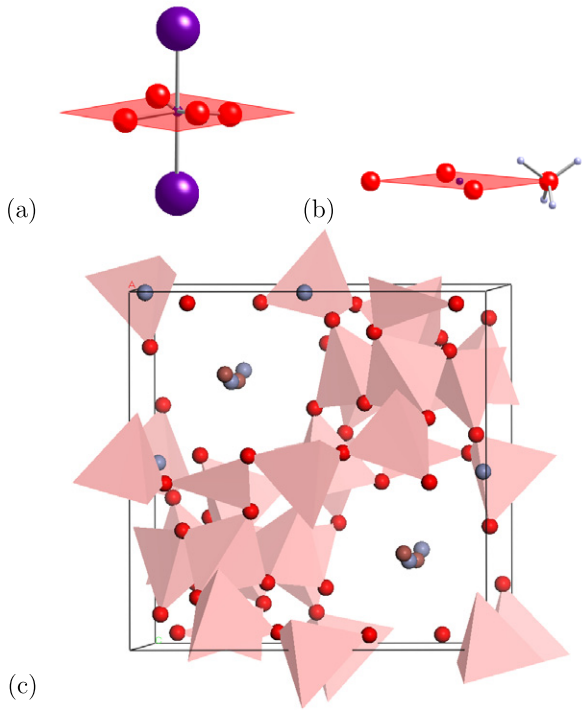

Figure 1. Crystal structure of boracite. A schematic picture of the M–X arrangement in cubic boracite is given in (a) and (b). Panel (a) shows the M atom at the centre of the graph surrounded by four O2 atoms that are located below and above a plane chosen so that it contains the M ion and the distances to the oxygen ions are minimal. X atoms are indicated by the large spheres. Panel (b) shows the O1 atoms at the corners of the above mentioned plane. Their tetrahedral coordination by B2 atoms (small spheres) is indicated in the right corner. The light grey polyhedra in (c) represents borate groups of orthorhombic Zn–Cl viewed nearly parallel to [001]. Boron atoms are either threefold planar or fourfold tetrahedrally coordinated by oxygen atoms and are not shown. There are channels in the structure containing –M–X–M–X–M– chains. In cubic boracite, the atoms in the chain are equidistant and the chains are linear. In low symmetry boracites, the distances to the neighbouring atoms along the chain are unequal and the chains have the form –X . . . M–X . . . M–X . . ., where . . . signifies a long distance and – a short distance. Also, in low symmetry boracites the chains are slightly kinked, and there are several symmetrically independent M–O distances.

(This figure is in colour only in the electronic version)

where $\alpha^{\mathrm{cp}} = 60°$ is the angle between the basic lattice vectors. The rhombohedral boracites discussed here have space group $R3c$ with lattice vectors

$$\boldsymbol{a}_1^{\mathrm{r}} = \boldsymbol{a}_1^{\mathrm{cp}}, \qquad \boldsymbol{a}_2^{\mathrm{r}} = \boldsymbol{a}_2^{\mathrm{cp}}, \qquad \boldsymbol{a}_3^{\mathrm{r}} = \boldsymbol{a}_3^{\mathrm{cp}} \tag{4}$$

and an angle $\alpha^{\mathrm{r}} \neq 60°$ in the rhombohedral setting (index r). Cell parameters in the hexagonal setting are obtained by

$$\boldsymbol{a}_1^{\mathrm{h}} = \boldsymbol{a}_1^{\mathrm{r}} - \boldsymbol{a}_2^{\mathrm{r}}, \qquad \boldsymbol{a}_2^{\mathrm{h}} = \boldsymbol{a}_2^{\mathrm{r}} - \boldsymbol{a}_3^{\mathrm{r}}, \qquad \text{and} \qquad \boldsymbol{a}_3^{\mathrm{h}} = \boldsymbol{a}_3^{\mathrm{r}} + \boldsymbol{a}_3^{\mathrm{r}} + \boldsymbol{a}_3^{\mathrm{r}}. \tag{5}$$

Neglecting changes in the magnitude of the lattice parameters, the shear deformation of the primitive cubic cell to the rhombohedral system is estimated by the rhombohedral scalar strain

$$e^{\mathrm{r}} = 3|\cos\alpha^{\mathrm{r}} - \cos\alpha^{\mathrm{cp}}|/\sin\alpha^{\mathrm{cp}} = 3|\cos\alpha^{\mathrm{r}} - \cos 60°|/\sin 60°. \tag{6}$$

While in the present study a number of boracites has been studied by model calculations, Co–Cl boracite has also been investigated experimentally. The structure of $Co_3[B_7O_{13}]Cl$ boracite has been determined by Ju *et al* (2002) from powder diffraction data. Some B–O bond lengths reported in that study (Ju *et al* 2002) are not easily reconciled with B–O distances observed in related compounds. Specifically, the interplanar distances in threefold-coordinated boron are expected to be significantly shorter than in the fourfold-coordinated boron. Data from quantum mechanical calculations on a wide variety of borates (Hantsch 2005) give values for the B–O bond of 1.329–1.416 Å for threefold, and 1.437–1.516 Å for fourfold coordination. Ju *et al* (2002), however, report a B–O distance of 1.436(7) Å for threefold coordination. Therefore, we redetermined the structure in order to clarify whether an unusual structural deformation was present.

A second part of the present investigation addresses the inconclusive results concerning the spontaneous deformation in Mg–Cl boracite. At ambient conditions, the crystal structure of Mg–Cl is orthorhombic with space group symmetry $Pca2_1$ and all atoms are located in the general position ($4a$) (Dowty and Clark 1972, 1973, Ito *et al* 1951). These authors report no orthorhombic spontaneous deformation at room temperature, i.e. the a_1^o and a_2^o lattice parameters agree to within the fourth decimal place. However, Torre *et al* (1972) found a small difference of about 9×10^{-3} Å between the a_1^o and a_2^o lattice parameters. Furthermore, they reported a ferroelastic interchange of the $\boldsymbol{a}_1^o$ and $\boldsymbol{a}_2^o$ axes on the application of an external stress (120 MN m^{-2}). As the agreement between the a_1^o and a_2^o lattice parameters corresponds to an accidental degeneracy and not a symmetry-related one, it is to be expected that a change in temperature or pressure will lift this accidental degeneracy. Neither temperature-dependent studies nor high pressure studies have been reported for Mg–Cl boracite up to now. It is straightforward to study pressure-induced structural changes with quantum mechanical atomistic model calculations and this has been done here after verifying that the model calculations are sufficiently accurate to investigate the small spontaneous deformations in boracites.

Furthermore, the self-consistent charge obtained from the quantum mechanical calculations can be analysed and compared to conventional crystal chemical reasoning based e.g. on electronegativities and ion sizes. This has been done here for a number of boracites in order to better understand the structure–property relations in this interesting group of materials.

In summary, the present study combines the results of powder diffraction experiments and quantum mechanical calculations based on density functional theory to complement the available information, and provide new insight into the bonding properties in boracites.

2. Experimental details

Deep-purple coloured crystals of Co–Cl were grown by a chemical vapour transport method (Schmid 1965) and characterized by optical microscopy, thermo-analysis and electron microscopy (Castellanos-Guzman *et al* 2000, 2001, Mendoza-Alvarez *et al* 1985).

The structure refinement from powder data was necessary due to the presence of multiple twinning in the crystals, caused by the above-mentioned ferro-elastic phase transitions. The crystals were ground in an agate mortar. X-ray powder diffraction data were collected with Mo radiation (Kα1, 0.7093 Å) due to the strong fluorescence and absorption of Co in experiments with Cu radiation. The sample was prepared in a glass capillary (0.2 mm diameter) and data were taken at a Stoe transmission diffractometer from 3 to 56° 2θ at a step width of 0.01°. The crystal structure was refined from the powder data by the Rietveld method applying the FULLPROF suite (Rodriguez-Carvajal 1998). The atomic coordinates given by Ju *et al* (2002) were used as starting values. The background was described by a

linear interpolation between 14 manually selected points and the peak profiles were modelled using a modified pseudo-Voigt function (Thompson *et al* 1987). The standard deviations of the refined parameters were scaled with the Bérar factor (Berar and Lelann 1991).

2.1. Computational details

The quantum mechanical calculations described here are based on density functional theory. In these calculations the Perdew–Burke–Ernzerhof version of the generalized gradient approximation (GGA) was employed (Perdew *et al* 1996). For these calculations we used academic and commercial versions of the CASTEP program, which is described elsewhere (Milman *et al* 2000, Payne *et al* 1992, Segall *et al* 2002).

In these calculations, ultrasoft pseudopotentials were used with a maximum cut-off energy of the plane waves of 380 eV. In addition to the cut-off energy, one further parameter determines the quality of the calculations, namely the density of points with which the Brillouin zone is sampled. The wavevectors for the sampling points were chosen according to the scheme proposed by Monkhorst and Pack (1976). Here, we use a sampling of the reciprocal space such that distances between grid points are less than 0.04 $Å^{-1}$. All structural parameters not constrained by the space group symmetry were relaxed for given pressures using a standard BFGS algorithm based on a Hessian in the mixed space of cell parameters and internal degrees of freedom. After the final self-consistency cycle the remaining stress was less than 0.02 GPa. The present calculations are restricted to the athermal limit, in which temperature effects and zero-point motions are neglected. For transition metal containing boracites spin polarized calculations were performed. Bond populations were obtained by a projection of the self-consistent electron density onto a minimal basis set.

3. Results and discussion

3.1. Trigonal boracite: the structure of Co–Cl

The result from the Rietveld refinement of Co–Cl is shown in figure 2. The agreement parameters for the whole pattern are $R_p = 3.23$, $R_{wp} = 4.07$, $R_B = 3.79$, and $\chi^2 = 1.05$. The cell parameters in the hexagonal setting are given in table 1. Table 2 contains the refined atomic coordinates and atomic displacement parameters. The atom labels and the origin of the unit cell are as for congolite, $Fe_{2.4}Mg_{0.6}[B_7O_{13}]Cl$ (Dowty and Clark 1973), with $z(Co) = 0.3235$ fixed.

The experimentally determined cell parameters agree well with the previously reported data of Ju *et al* (2002) (table 1). The deviations are 0.03% in a_1 and 0.01% in a_3. The cell parameters from the quantum mechanical calculations (table 1) are larger by about 1% than the experimental values. This corresponds to the generally observed systematic deviation for DFT-GGA calculations and has been observed for all other compositions and pressures discussed below.

Selected bond lengths are collected in table 3. In contrast to the findings of Ju *et al* (2002), both the present experimental and theoretical data show a distinct difference in the B–O bond lengths for boron in three- or fourfold coordination, where the bonds for three-coordinated boron are significantly shorter than for four-coordinated boron. This is generally observed in single crystal structure refinements of borates as well as in quantum mechanical calculations (e.g. Hantsch 2005).

Tables 1 and 3 also show a very good agreement between the experimentally determined and the calculated structural parameters of Co–Cl. The scatter between the observed and calculated bond lengths is small (figure 3). The unusual bond length for B3–O21 = 1.436(7) Å reported by Ju *et al* (2002) could not be confirmed.

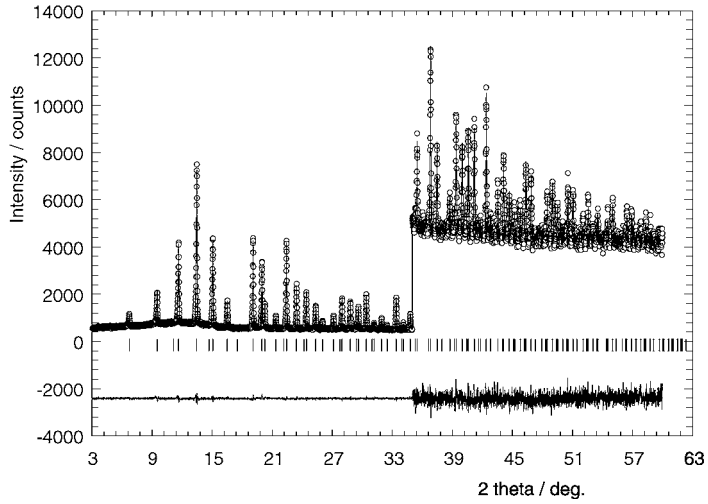

Figure 2. X-ray powder diffraction pattern from Co–Cl boracite. Circles correspond to experiment data; the line running through the data points is from the Rietveld refinement. Vertical markers indicate the positions of the Bragg peaks. The difference between observed and calculated data is given by the curve below the data points, which has been offset for clarity. Intensity values for 2θ values above 34° are scaled by 10.

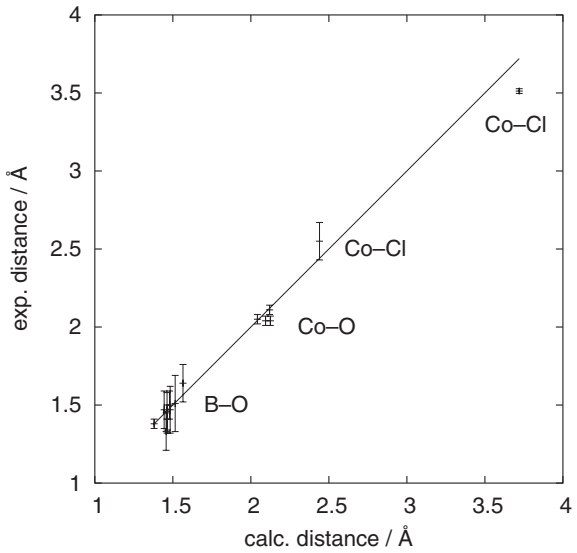

Figure 3. Calculated versus experimentally determined bond lengths in Co–Cl. The line represents perfect agreement.

3.2. Trigonal boracites: spontaneous deformation

We have computed the structures of a number of boracites in order to determine whether the accuracy of the present DFT-GGA calculations is sufficient to reproduce the small distortions in the non-cubic boracites. The rhombohedral distortion is defined above (equation (6)), and for Co–Cl, Mg–F, Zn–F and Zn–Cl the corresponding values are listed in table 1. The

Table 1. Cell parameters and lattice strain for Mg–F, Mg–Cl, Co–Cl, Co–I, Cu–Cl, Cu–I, Zn–F, Zn–Cl, Zn–I, and Zn–Br boracite at ambient pressure, determined experimentally from Rietveld refinement (X), obtained from quantum mechanical calculations (DFT), and from the literature. Strain values in italics correspond to orthorhombic unit cells with $a_2 < a_1$.

			Cell parameters (Å)			
	Symmetry	Note	a_1	a_2	a_3	Strain $\times 10^3$
Mg–F	$R3c$	DFT	8.582 91		21.424 90	43.369
		[g]	8.480 4		21.086 4	34.447
Mg–Cl	$Pca2_1$	DFT	8.675 71	8.662 32	12.272 79	*3.090*
		[h]	8.549 6(6)	8.549 6(6)	12.091 0(9)	0.000
		[i]	8.541 69(4)	8.550 49(3)	12.097 74(4)	2.059
Mg–Cl	$F\bar{4}3c$	DFT	12.213 68			
		[d]	12.098 6(2)			
Co–Cl	$R3c$	X	8.548 8(1)		20.966 1(6)	2.853
		DFT	8.646 47		21.205 40	2.828
		[a]	8.550 7(1)		20.968 5(1)	2.607
Co–I	$F\bar{4}3c$	DFT	11.989 13			
		[b]	12.119(3)			
Cu–Cl	$Pca2_1$	DFT	8.602 06	8.551 95	12.114 56	*11.685*
Cu–I	$R3c$	DFT	8.572 08		21.336 70	36.839
Cu–I	$F\bar{4}3c$	DFT	12.157 035			
		[c]	12.020 3(7)			
Zn–F	$R3c$	DFT	8.568 17		21.389 10	43.477
		[f]	8.497 02		21.161 40	43.478
Zn–Cl	$Pca2_1$		8.640 83	8.654 68	12.227 16	3.202
Zn–Cl	$R3c$	DFT	8.622 3		21.227 4	11.674
		[e]	8.537 25(7)		20.968 49(25)	6.232
Zn–I	$Pca2_1$	DFT	8.702 76	8.700 99	12.306 47	*0.408*
Zn–Br	$Pca2_1$	DFT	8.658 37	8.675 55	12.257 26	3.963
		[j]	8.550 6(2)	8.559 9(2)	12.099 4(2)	*2.174*

[a] Ju *et al* (2002).
[b] Nelmes and Hay (1981).
[c] Berset *et al* (1985).
[d] Sueno *et al* (1973).
[e] Mao *et al* (1991).
[f,g] Bither and Young (1974).
[h] Dowty and Clark (1972, 1973).
[i] Torre *et al* (1972).
[j] Campa-Molina *et al* (2006).

spontaneous strains derived from the calculations are compared to experimentally determined ones in figure 4, where values for orthorhombic boracites have also been included. Given that the absolute values for the strains are rather small, it is gratifying to see that the DFT calculations are sufficiently accurate to reproduce spontaneous deformations and hence can be used to predict structure–property relations.

3.3. Orthorhombic boracites

It has been mentioned above that a number of boracites transform from the cubic phase into an orthorhombic phase with space group $Pca2_1$. In fact, the mineral after which the boracite family has been named is orthorhombic Mg–Cl boracite. There is an inconclusive discussion as to whether or not Mg–Cl boracite shows a spontaneous deformation at ambient conditions. Dowty and Clark (1972, 1973) did not detect any spontaneous deformation in their single

Table 2. Atomic coordinates and displacement parameters for Co–Cl. Values obtained from structure refinement of the powder diffraction data (X) are compared to the results of the *ab initio* calculations (DFT) and data from literature (Lit. = Ju *et al* (2002)).

Atom	Note	x/a	y/b	z/c	B(iso)
Co1	X	0.149(2)	0.296 8(3)	0.3235 (fixed)	0.92(3)
	DFT	0.144 00	0.290 66	0.3235	
	Lit.	0.148 9(7)	0.298 5(1)	0.325 0(1)	0.62(2)
Cl1	X	0.0	0.0	0.261 7(5)	1.8(2)
	DFT	0.0	0.0	0.271 46	
	Lit.	0.0	0.0	0.262 9(1)	2.1(2)
B1	X	0.170(8)	0.842(9)	0.079(1)	1.1(2)
	DFT	0.163 51	0.835 22	0.080 19	
	Lit.	0.167(3)	0.835(3)	0.079 9(8)	1.2(2)
B2	X	0.119(7)	0.901(7)	0.973(1)	1.1(2)
	DFT	0.101 36	0.897 22	0.968 25	
	Lit.	0.089(3)	0.895(3)	0.973 4(6)	1.2(2)
B3	X	0.0	0.0	0.098(2)	1.1(2)
	DFT	0.0	0.0	0.101 07	
	Lit.	0.0	0.0	0.096 7(9)	1.2(2)
O1	X	0.0	0.0	0.986(1)	0.37(7)
	DFT	0.0	0.0	0.984 09	
	Lit.	0.0	0.0	0.989 1(5)	0.25(4)
O21	X	0.837(2)	−0.004(2)	0.104(1)	0.37(7)
	DFT	0.840 18	−0.000 75	0.103 42	
	Lit.	0.834 9(9)	0.005 3(9)	0.098 9(4)	0.25(4)
O22	X	0.284(2)	0.253(3)	0.963(1)	0.37(7)
	DFT	0.289 67	0.261 44	0.960 18	
	Lit.	0.288(1)	0.262(2)	0.961 9(4)	0.25(4)
O23	X	0.198(2)	0.983(2)	0.909(8)	0.37(7)
	DFT	0.201 48	0.976 65	0.909 35	
	Lit.	0.197(1)	0.977(1)	0.909 1(4)	0.25(4)
O24	X	0.687(2)	0.765(2)	0.018 7(8)	0.37(7)
	DFT	0.695 23	0.774 25	0.018 72	
	Lit.	0.693(1)	0.771 5(9)	0.018 0(4)	0.25(4)

Table 3. Selected bond lengths (in Å) of Co–Cl from Rietveld refinement. The estimated standard deviations are given in parentheses. Values without esd are from the quantum mechanical calculations.

B1–	O21	1.51(6)	B2–	O1	1.64(4)	B3–	O21 (3×)	1.38(1)
		1.515			1.565			1.380
	O22	1.46(4)		O22	1.47(4)			
		1.463			1.444			
	O23	1.47(5)		O23	1.50(3)			
		1.483			1.479			
	O24	1.41(3)		O24	1.33(4)			
		1.463			1.457			
Co–	Cl	2.550(4)	Co–	O21	2.04(1)	Co–	O23	2.05(1)
		2.440			2.094			2.042
	Cl	3.512(5)		O22	2.11(1)		O24	2.04(1)
		3.720			2.120			2.125

crystal experiments on untwinned samples, while the measurements of Torre *et al* (1972) gave a spontaneous deformation of 2.059×10^{-3} according to equation (2).

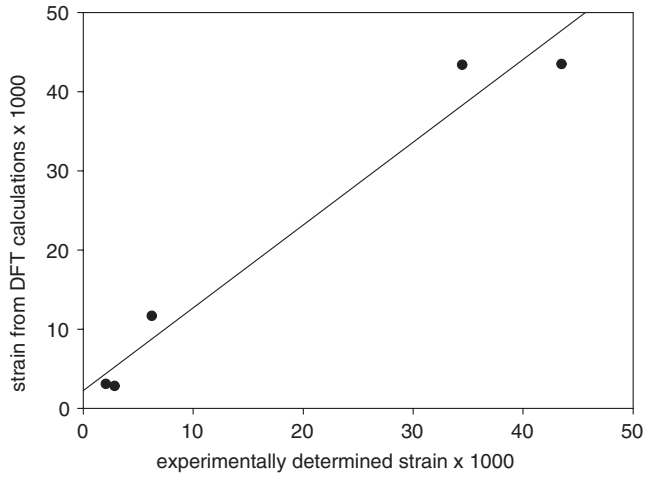

Figure 4. Comparison of the spontaneous strains obtained from experiment and calculated in the present study. Considering that the absolute distortions of the lattices are rather small, the agreement is very good.

Table 4. Pressure dependence of the cell parameters and the orthorhombic lattice strain of Mg–Cl boracite, calculated by DFT in space group $Pna2_1$. Strain values printed in italics represent values for $a_1 > a_2$.

p (Gpa)	a_1 (Å)	a_2 (Å)	a_3 (Å)	Strain $e^o \times 10^3$
1	8.652 018	8.641 513	12.241 583	*2.43*
2	8.628 772	8.622 116	12.212 649	*1.54*
5	8.562 955	8.564 991	12.128 121	0.47
10	8.458 331	8.482 449	11.999 510	5.69

The current DFT calculations support the finding of Torre *et al* (1972), in that the calculations give a small orthorhombic distortion of $e^o = 3 \times 10^{-3}$. The calculated enthalpies show that orthorhombic Mg–Cl boracite is more stable by ∼3 kJ mol^{-1} in the athermal limit than the cubic polymorph. This small difference is close to the accuracy of the calculations, and consistent with the comparatively low transition temperature (538 K). Notably, in the athermal limit the volume of the high temperature cubic primitive cell is smaller (911 Å^3) than that of the orthorhombic phase (922 Å^3).

3.3.1. High-pressure behaviour of orthorhombic Mg–Cl boracite. To date, no high pressure structural studies of boracites have been published and hence the pressure dependences of the spontaneous deformations of boracites are unknown. As the calculations described above have shown that the spontaneous deformation is well described by DFT calculations, we predict the behaviour of orthorhombic Mg–Cl boracite. The corresponding lattice parameters and the strain according to equation (2) are given for pressures of 1, 2, 5, and 10 GPa for Mg–Cl in table 4.

The volume bulk modulus for Mg–Cl $b_0 = 126.5(6)$ GPa was determined from the fit of a second order Birch–Murnaghan equation of state (Birch 1978), BM2, to the volume/pressure data. The fitted volume at zero pressure is $V_0 = 922.4(2)$ Å^3. The bulk modulus is similar to the values of framework silicates (with the exception of structures having rigid unit modes,

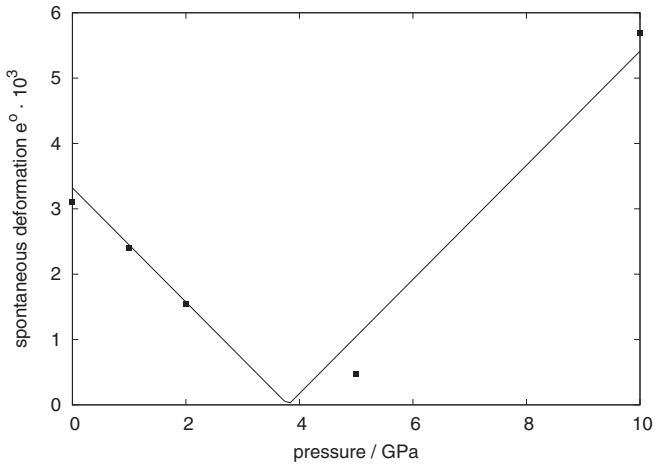

Figure 5. Pressure dependence of the idealized tetragonal spontaneous strain e_o for Mg–Cl. The line is a guide to the eyes.

such as quartz (Angel *et al* 1997) or moganite (Hantsch *et al* 2005)) or other 'framework-like' structures, such as the oxonitridosilicates (Friedrich *et al* 2005). From the fit of the BM2 to the cube of the individual cell parameters, values of the linear compressibility were determined: $k \parallel a_1 = 0.002\,93$, $k \parallel a_2 = 0.002\,38$, and $k \parallel a_3 = 0.002\,57$ GPa^{-1}. They show a small elastic anisotropy with the largest compressibility along the $\boldsymbol{a}_1$- and the smallest compressibility along the $\boldsymbol{a}_3$-direction of the orthorhombic lattice.

The spontaneous lattice deformation at zero pressure with respect to a metrically tetragonal lattice is ca. 0.003. It shows an interesting pressure dependence, with $e^o = 0$ at about 4 GPa (figure 5). This suggests a metrically tetragonal phase at this pressure. Above 4 GPa the crossover of the $\boldsymbol{a}_1$ and $\boldsymbol{a}_2$ lattice parameters causes a change of the sign of the strain. The reversal of these lattice parameters was also observed experimentally by Torre *et al* (1972) for the application of a uniaxial stress. A similar effect was mentioned by Nelmes (1974), who reviewed a transition in Fe–I boracite from orthorhombic to monoclinic symmetry through an accidentally cubic metric.

The compression mechanism for Mg–Cl is analysed from the data sets at 0 and 10 GPa. The changes of the B–O bond lengths and of the O–B–O angles are in the order of less than 1%. The tetrahedra tend to become more ideal. The major changes are observed for the B–O–B angles, which decrease by 2%. Significant changes are also found for the M–X distances. While the short distance (2.614 Å) decreases by about 2%, the long distance (3.547 Å) decreases by 3%. The M–O distances are shortened by less than 0.1 Å.

3.4. Cubic boracites

Table 1 also lists the calculated cell parameters for cubic Co–I, Cu–I, and Mg–Cl boracites. They agree well with the experimental observations. Selected bond lengths and angles are given in table 5. The general agreement between experiment and calculations is very good. Note that Cu–I has not yet been synthesized. However, its hypothetic crystal structure shows no peculiarities compared to the experimentally determined structures of Mg–Cl or Co–I.

The influence of the exchange of either M or X on the BO network is negligibly small. We observe two geometrically distinct B sites. While B1 is surrounded by oxygen in the

Table 5. Selected interatomic distances and angles in the cubic boracites Mg–Cl, Co– and Cu–I derived from the quantum mechanical calculations (left) and experimental data from literature (right). The references are Sueno *et al* (1973) for Mg–Cl and Nelmes and Hay (1981) for Co–I.

		Mg–Cl	Co–I	Cu–I
d(B1–O2) (Å)	4×	1.477/1.472	1.472/1.463	1.476
d(O2–O2) (Å)	3×	2.405/2.382	2.396/6 × 2.389	2.409
	3×	2.425/2.444	2.420	2.413
∠(O2–B1–O2) (deg)	4×	109.0/108.1	108.9/6 × 109.47	109.4
	2×	110.4/112.2	110.5	109.7
d(B2–O1) (Å)	1×	1.702/1.693	1.681/1.673	1.700
d(B2–O2) (Å)	3×	1.440/1.437	1.437/1.435	1.441
d(O1–O2) (Å)	3×	2.521/2.519	2.475/2.490	2.501
d(O2–O2) (Å)	3×	2.392/2.383	2.408/2.386	2.407
∠(O1-B2-O2) (deg)	3×	106.4/106.9	104.8/106.2	105.3
∠(O2–B2–O2) (deg)	3×	112.3/111.9	113.7/112.5	113.3
oop (Å)		0.400/0.418	0.366/0.402	0.380
d(M–X) (Å)	2×	3.053/3.025	2.997/3.030	3.005
d(M–O2) (Å)	4×	2.066/2.023	1.998/2.056	2.008

geometry of an almost perfect tetrahedron, the B2 site shows an OBO_3 environment. In contrast to the ideal tetrahedron found by Nelmes and Hay (1981) for Co–I, the calculation shows a deformation as observed for Mg–Cl. The B2 boron atom is displaced from the centre of the coordination polyhedron towards the three O2 atoms with the out of plane distance (oop) given in table 5. However, the coordination polyhedron formed from the four oxygen atoms can still be considered a distorted tetrahedron.

3.5. Discussion of bonding properties

The results of the quantum mechanical calculations can be used to further understand the similarities and differences in the bonding in the various boracites. Here, we attempt to establish a correlation between the properties of the M and X ions and the interaction between them, and analyse the strength of the B–O interactions.

To characterize the B–O interactions, we have analysed the bond populations along the B–O contacts. A typical dependence of this bond population is shown in figure 6 for cubic and orthorhombic Mg–Cl boracite, where for the latter two sets of data, obtained for the 0 and 10 GPa structures, are shown. The bond populations decrease linearly with increasing B–O distance for these three data sets. We have then confirmed this behaviour in the other boracites studied here, including those having long B–O distances of about 1.7 Å. In all cases, we found the same dependence: the bond populations are always about 0.8 e Å^{-3} for the short (∼1.4 Å) bonds and decrease to about 0.4 e Å^{-3} for the long B–O bonds. This clearly shows that the character of the B–O bonds is essentially independent of the metal and halogen ions. It also indicates that phase transitions are not due to some discontinuity in the B–O bonding on distortion.

A description of the character of the M–O interactions is not as straightforward. In the cubic boracites, the M atoms are surrounded by four O2 atoms at equal distance and two equidistant X atoms, resulting in a MO_4X_2 complex. In the low symmetry boracites, the distances become inequivalent, as has been discussed before. Figure 7 shows the dependence of the bond population on the M–O distances for the various boracites, and clearly the bonding character is not a simple function of distance. A first distinction can be made between the

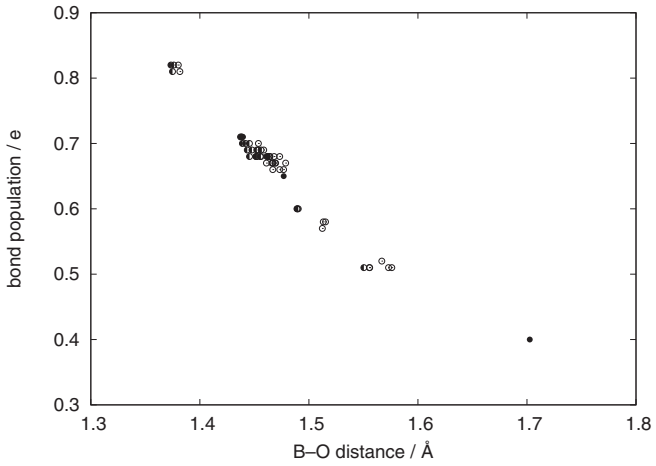

Figure 6. Dependence of the bond population in Mg–Cl boracite with cubic (0 GPa, filled circles) and orthorhombic symmetry at 0 GPa (open circles) and 10 GPa (half filled circles) on the B–O bond length.

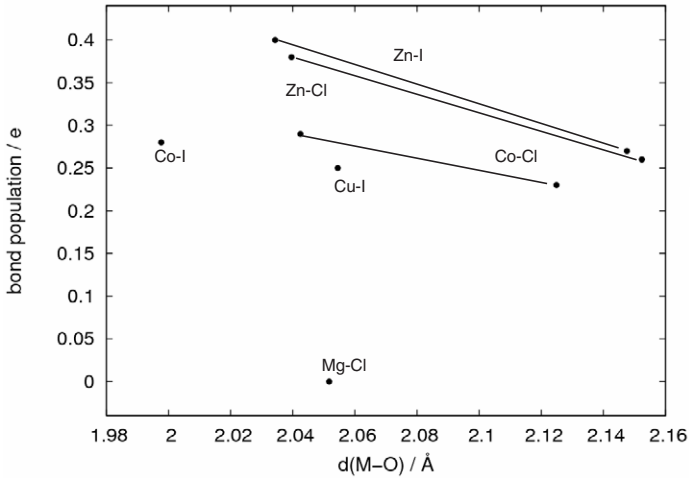

Figure 7. Bond population as a function of the M–O bond length (Å) in boracites. Lines connect extreme values of the corresponding M–O bonds.

transition metal containing boracites and Mg–Cl boracite. The sum of the ionic radii for Mg^{2+} and O^{2-} is about 1.92–2.07 Å (Shannon 1976), depending on the choice of the coordination of the Mg^{2+}. In Mg–Cl boracite, the experimentally determined distances are d(M–O) $\sim$ 2.03 Å, i.e. very close to the sum of the ionic radii. The analysis of the charge density shows that there is no charge accumulation along this contact and hence there is no covalent contribution to the Mg–O interaction. In contrast to the Mg–O bond in Mg–Cl boracite, the M–O bonds in the transition metal containing boracites are all rather similar and show an appreciable bond population, which indicates that they are significantly more covalent than the Mg–O bond in Mg–Cl boracite. This is qualitatively consistent with a conventional analysis based on Pauling's electronegativities, where the difference in the electronegativities of Mg and O ($\Delta = 2.13$) is conventionally taken to indicate ionicity of the bond of about 70%, while the electronegativity

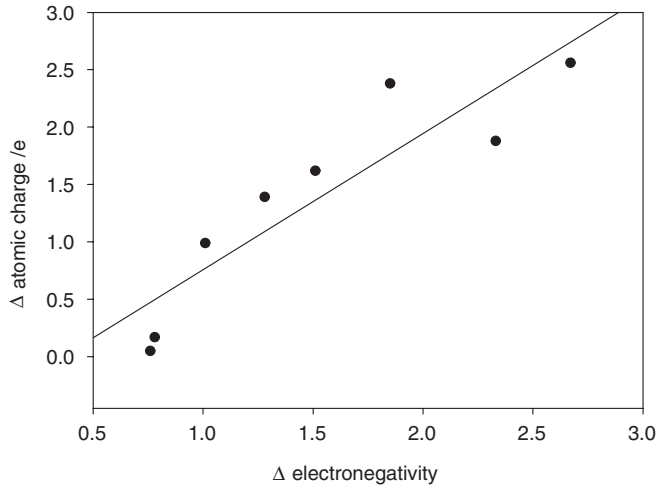

Figure 8. Correlation between the difference between the atomic charges of the M and X atoms in boracite derived from the quantum mechanical calculations and the difference between the electronegativities of the M and X ions. The line represents the result of a least squares fit of a linear relationship.

differences in the transition metal containing halogenide boracites are smaller (e.g., for Co containing compounds, $\Delta = 1.56$, equivalent to 47% ionic character of the bond) and hence should be more covalent. Such an analysis gives an increasing ionicity for the M–O bonds according to the sequence Cu $\sim$ Co $>$ Zn $>$ Mg. We calculate a very similar bond population of the M–O bond for all transition metal boracites, which implies that the simple analysis based only on the electronegativity differences of the M and O ion is insufficient and that the character of the M–O bonds is influenced by the two halogen neighbours.

The bond populations between the M and the X ions are either small or zero, and do not show any systematic relations. However, a more detailed analysis reveals some interesting relationships. It has been mentioned above that during the phase transformations M–X pairs are formed, which are linked by long M . . . X distances. As there was no charge accumulation for either the long or the short contacts, the atomic arrangement is likely to be determined by electrostatic interactions. One expects that the difference in electronegativities of the M and the X ions will lead to charge transfer within the chain. We confirm this by a plot of the atomic charges as derived from a Mulliken population analysis as a function of the difference of the electronegativity of the M and X ions (figure 8). Here, the extreme case is Mg–F boracite, where the electronegativity difference is 2.67, while the atomic charges are $+1.79$ and -0.77 e, for Mg and F, respectively, which is very close to their formal charges. The other extreme is Cu–I, in which in fact a detailed analysis of the charge density difference maps show that there is some small charge accumulation between the Cu and the I (similar to Co–I), so that an integration of the total charge around iodine actually gives a slightly positive total atomic charge.

After having established that the difference in Pauling's electronegativity is correlated to the charge distribution, the next step is to show that this is correlated to the distances in and between the M–X pairs. Figure 9 shows that this is the case for the dependence of the short distance on the electronegativity difference. A similar plot, albeit with a positive slope, can be constructed for the dependence of the long distance on the electronegativity difference. In fact, the short and long distances are very well correlated (figure 10), and hence it now seems possible to predict the interchain distances from the electronegativity differences. Interestingly,

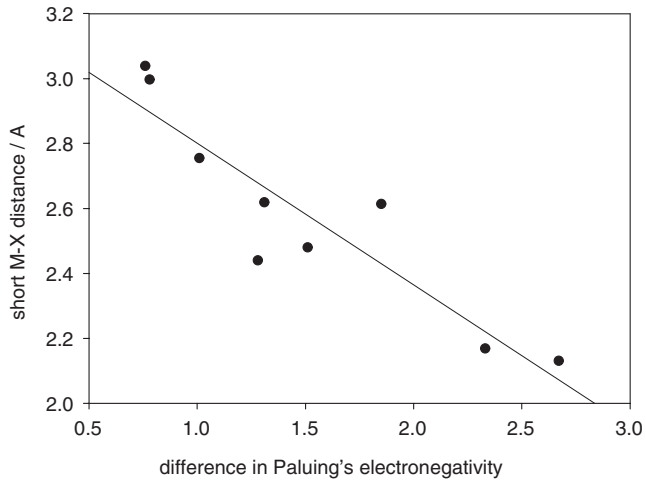

Figure 9. Dependence of the short intrapair distance M–X on the difference of the electronegativity. The larger the difference, the shorter the M–X bond. Conversely, the interpair distance X . . . M increases with an increasing difference of the electronegativity.

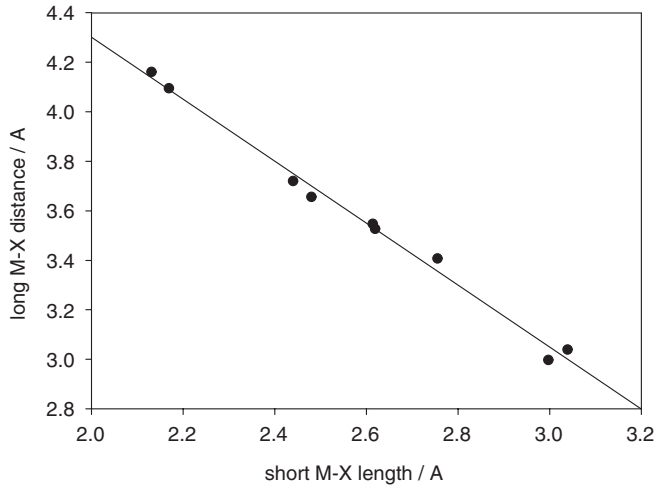

Figure 10. Correlation between the distance in the M–X pairs and between the M–X pairs for halogenide boracites. The slope of the line, which represents a least square fit to the data, is −1.25. This implies that the chain length is not constant (which would correspond to a slope of −1), but rather that in cubic boracites with M–X values around 3.0 the chains are shortest, while in those boracites with short M–X distances, which occur in boracites in which the ions are highly charged, the sum of the inter and intra-pair distances is longest.

the chain lengths as computed from the sum of the long and short distances is not constant, but the sum increases significantly with increasing charge transfer. In a last step, we plot the spontaneous deformations as a function of the electronegativity difference. Here, we see a more complex behaviour (figure 11), which, however, seems to describe all boracites reasonably well. Clearly, the database is currently still limited and the conclusions drawn here are therefore to some extent still tentative. Specifically, the plot suggests that there may be a maximal strain of about 0.045. Clearly, more data points will be required to characterize the dependence of

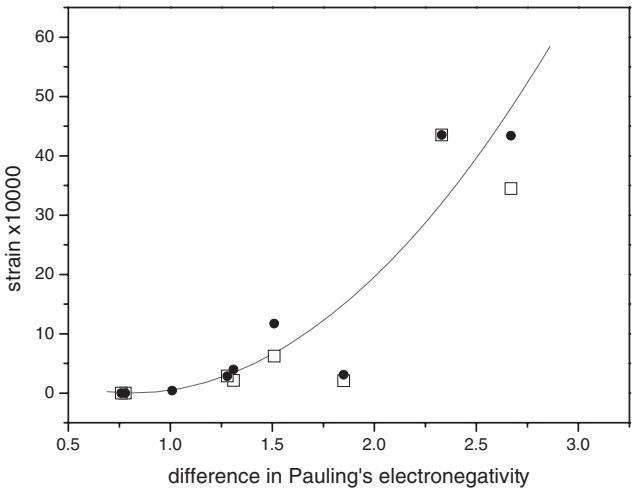

Figure 11. The computed spontaneous deformation (filled circles, DFT data; open squares, experimental data) is correlated to the difference of the electronegativities of the M and X ions. The line is a guide to the eye.

the strain on the electronegativity difference more clearly. However, DFT theory calculations on the transition metal halogenide boracites, both existing and hypothetical ones, only take a few days on a computer cluster of moderate size, and hence this analysis can be extended. It is maybe worthwhile to emphasize that the DFT calculations simplify this analysis, in that all calculations refer to the same athermal ground state, and hence need not be normalized with respect to transition temperatures.

4. Summary and conclusions

In the current study, x-ray powder diffraction experiments and density functional theory based calculations have been used to study the structure and bonding of halogenide boracites. We have shown that the small spontaneous deformations of non-cubic boracites are reproduced satisfactorily by DFT calculations and that the bonding properties of the B–O bond system are essentially unaffected by a substitution of the halogen or metal ions. The distances in the M–X chains can be rationalized in terms of the difference in the electronegativities of the metal and halogen ions. Large differences in the electronegativities lead to large charge transfers from the X anion to the cation and short M–X distances, while in those cases where the difference in the electronegativities are small, the M and X are more equally spaced along the chains. We have predicted the compressibility of Mg–Cl boracite and found that it corresponds to values found for framework silicates.

Acknowledgments

We wish to thank Alexandra Lieb from the Chemistry Department of the LMU Munich for recording the powder diffraction pattern. This work was supported by the German Science Foundation DFG and the Mexican Science Council (CONACYT contract No. 34959E) and DAI.

References

Angel R J, Allan D R, Miletich R and Finger L W 1997 The use of quartz as an internal pressure standard in high-pressure crystallography *J. Appl. Crystallogr.* **30** 461–6

Berar J F and Lelann P 1991 E.s.d.'s and estimated probable error obtained in Rietveld refinements with local correlations *J. Appl. Crystallogr.* **24** 1–5

Berset G, Depmeier W, Boutellier R and Schmid H 1985 Structure of boracite $Cu_3B_7O_{13}I$ *Acta Crystallogr.* A **41** 1694–6

Birch F 1978 Finite strain isotherm and velocities for single-crystal and polycrystalline NaCl at high pressure and 300 K *J. Geophys. Res.* **83** 1257–68

Bither T A and Young H S 1974 Nitrato- and fluoroboracites $M_3B_7O_{13}NO_3$ and $M_3B_7O_{13}F$ *J. Solid State Chem.* **10** 302–11

Campa-Molina J, Ulloa-Godinez S, Barrera A, Bucio L and Mata J 2006 Nano and micro reoriented domains and their relation with the crystal structure in the new ferroelectric boracite $Zn_3B_7O_{13}Br$ *J. Phys.: Condens. Matter* **18** 4827–37

Castellanos-Guzman A G, Czank M, Kumar A, Singh G, Tiwari V S and Wadhawan V K 2000 Optical and electron microscopy of the domain structure of $Co_3B_7O_{13}Cl$ ferroelectric/ferroelastic boracite *The 6th Int. Symp. on Ferroic Domains and Mesoscopic Structure (Nanjing, China)*

Castellanos-Guzman A G, Czank M, Kumar A, Singh G, Tiwari V S and Wadhawan V K 2001 Calorimetric, optical and electron microscopy studies of $Co_3B_7O_{13}Cl$ ferroic boracite *Ferroelectrics* **251** 61–8

Dowty E and Clark J R 1972 Atomic displacements in ferroelctric trigonal and orthorhombic boracite structures *Solid State Commun.* **10** 543–8

Dowty E and Clark J R 1973 Crystal-structure refinements for orthorhombic boracite, $Mg_3B_7O_{13}Cl$, and a trigonal, iron-rich analogue *Z. Kristallogr.* **138** 64–99

Dvorak V 1971 A thermodynamic theory of the cubic–orthorhombic phase transition in boracites *Czech. J. Phys.* B **21** 1250–61

Dvorak V and Petzelt J 1971 Symmetry aspects of the phases transitions in boracites *Czech. J. Phys.* B **21** 1141–52

Friedrich A, Knorr K, Lieb A, Rath S, Hanfland M, Winkler B and Schnick W 2005 Bulk modulus and phase transition of the oxonitridosilicate chloride $Ce_4[Si_4O_{3+x}N_{7-x}]Cl_{1-x}O_x$, $x = 0.2$ at high pressures up to 28 GPa *Z. Kristallogr.* **220** 245–9

Hantsch U 2005 Quantenmechanische Rechnungen an idealen Kristallen und an Kristallen mit Strukturgradienten *PhD Thesis* Johann Wolfgang Goethe University, Frankfurt (Main)

Hantsch U, Winkler W, Pickard C J, Gale J D, Warren M C, Milman V and Mauri F 2005 Theoretical investigation of moganite *Eur. J. Mineral.* **17** 21–30

Ito T, Morimoto N and Sadanaga R 1951 The crystal structure of boracite *Acta Crystallogr.* **4** 310–6

Ju J, Li H, Wang Y, Lin J and Dong C 2002 A novel synthesis approach to transition metal boracites *J. Mater. Chem.* **12** 1771–4

Mao S Y, Mendoza-Alvarez M E, Depmeier W, Kubel F and Schmid H 1991 Structure refinement of trigonal zinc–chlorine boracite, $Zn_3B_7O_{13}Cl$, from single-crystal and powder x-ray diffraction *Ferroelectrics* **115** 91–6

Mendoza-Alvarez M-E, Rivera J P and Schmid H 1985 Optical, electric and dielectric studies of cobalt–chlorine boracite, $Co_3B_7O_{13}Cl$ *6th Conf. on Ferroelecricity (Kobe)*; *Japan. J. Appl. Phys.* (suppl.) **24-2** 1057–9

Milman V, Winkler B, White J A, Pickard C J, Payne M C, Akhmatskaya E V and Nobes R H 2000 Electronic structure, properties, and phase stability of inorganic crystals: a pseudopotential plane-wave study *Int. J. Quantum Chem.* **77** 895–910

Monkhorst H J and Pack J D 1976 Special points for Brillouin-zone integrations *Phys. Rev.* B **13** 5188–92

Nelmes R J 1974 Structural studies of boracites. A review of the properties of boracites *J. Phys. C: Solid State Phys.* **7** 3840–54

Nelmes R J and Hay W J 1981 Structural studies of boracites-VI. The cubic phase of cobalt iodine boracite, $Co_3B_7O_{13}I$, and of copper bromine boracite $Cu_3B_7O_{13}Br$ *J. Phys. C: Solid State Phys.* **14** 5247–57

Payne M C, Teter M P, Allan D C, Arias T A and Joannopoulos J D 1992 Iterative minimization techniques for *ab initio* total-energy calculations: molecular dynamics and conjugate gradients *Rev. Mod. Phys.* **64** 1045–97

Perdew J P, Burke K and Ernzerhof M 1996 Generalized gradient approximation made simple *Phys. Rev. Lett.* **77** 3865–8

Rodriguez-Carvajal J 1998 *FULLPROF 3.5d.* LLB Saclay

Schmid H 1965 Die Synthese von Boraziten mit Hife von chemischen Transportreaktionen *J. Phys. Chem. Solids* **26** 973–6

Segall M D, Lindan P L D, Probert M J, Pickard C J, Hasnip P J, Clark S J and Payne M C 2002 First-principles simulation: ideas, illustrations and the CASTEP code *J. Phys.: Condens. Matter* **14** 2717–44

Shannon R 1976 Revised effective ionic radii and systematic studies of interatomic distances in halides and chalcogenides *Acta Crystallogr.* C **32** 751–67

Sueno S, Clark J R, Papike J J and Konnert J A 1973 Crystal-structure refinement of cubic boracite *Am. Mineral.* **58** 691–7

Thompson P, Cox D E and Hastings J B 1987 Rietveld refinement of Debye–Scherrer synchrotron x-ray data from Al_2O_3 *J. Appl. Crystallogr.* **20** 79–83

Toledano P, Schmid H, Clin M and Rivera J P 1985 Theory of the low temperature phases in boracites: latent antiferromagnetism, weak ferromagnetism, and improper magnetostructural couplings *Phys. Rev.* B **32** 6006–38

Torre O P, Abrahams S C and Barns R L 1972 Ferroelectric and ferroelastic properties of Mg–Cl boracite *Ferroelectrics* **4** 291–8